Noise Analysis and Performance Comparison of Low Current Measurement Systems for Biomedical Applications

Dongsoo Kim, *Member, IEEE*, Brian Goldstein, *Graduate Student Member, IEEE*, Wei Tang, *Student Member, IEEE*, Fred J. Sigworth, and Eugenio Culurciello, *Senior Member, IEEE*

***Abstract*—In this paper, we report on the noise analysis of low current measurement systems for biomedical applications and their fundamental limits. We analyzed resistive feedback, capacitive feedback and current amplifier circuits for low current measurement systems. Detailed noise analysis for different biomedical applications are presented and matched with measurement data using a 0.5-μm fabrication process. Based on the theoretical analysis and the corresponding measurement results, the capacitive feedback system provides better noise performance for the measurement of low current than the others. The capacitive feedback circuit is capable of measuring 750 fA RMS at a 10 kHz sampling rate, whereas the resistive feedback provides 4 pA and the current conveyor provides 600 pA at the same bandwidth. This paper provides design guidelines to maximize the performance of low current measuring system for biomedical instrumentation and to provide the best performance available with CMOS technologies.**

***Index Terms*—Biomedical measurements, capacitive feedback, current conveyor, current measurement, integrator, low current measurement system (LCMS), low noise circuit, noise analysis, resistive feedback.**

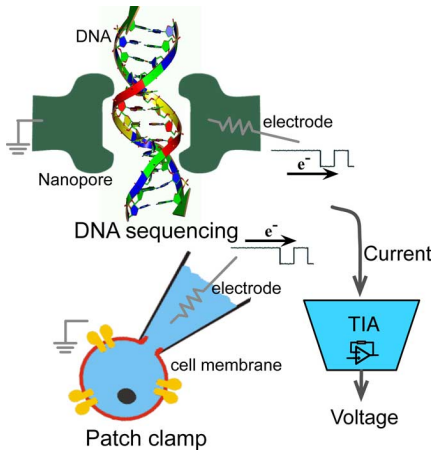

Fig. 1. Examples of biomedical applications include DNA sequencing and patch-clamping using low current measurement systems. All of these applications, together with nanoscience large-scale arrays, need to record $\pm 1 - 100$ pA currents at 10 kHz or more.

I. Introduction

INTEGRATED current measurement systems are becoming extremely important integrated circuit components to interface and study physical phenomena at the sub-micro-scale and also for biological research and instrumentation [1]. All of these current measurements require a compact instrumentation head-stage with very low input current noise. For example, to measure ion channel and membrane protein currents as shown in Fig. 1, an integrated low current measurement system with pico-ampere resolution is required, such as commercial patch-clamp amplifiers which can measure a cell membrane's conductance and are normally used to study the effect of drugs and medical treatments on ion channel dynamics. In individual ion-channels, currents of ± 5 pA are typical. Patch-clamp experiments require recording bandwidths of 1 to 10 kHz. Another example of a low current measurement system (LCMS) is one used in DNA sequencing with a nanopore [2], [3]. When the nanopore is immersed in a conducting fluid and a potential difference is applied across it, the conduction of ions through the nanopore generates an electric current. When individual DNA bases, delivered by an enzyme, pass through the nanopore, they modulate the current through the nanopore, with a range of 10–50 pA. These currents are usually recorded at 10 kHz. Another application where a LCMS is used is in large-scale nanosensing devices [4], where low chemical and biological concentrations translate in pico-ampere to tens of nano-ampere level currents that need to be measured at high rates. The 10 kHz bandwidth mentioned is a lower-bound compromise in order to achieve less noise in the measurement, as more bandwidth is always desired when possible. Several low current measurement systems have been implemented and published in the literature [5]–[13]. Low current measurements can be performed with passive components in shunt or feedback configuration with respect to an active amplifier. For practical reasons, low current measurements can be conducted with capacitors or resistors as passive

Manuscript received July 08, 2011; revised October 18, 2011; accepted March 16, 2012. This work was supported by the IEEE, and in part by NSF Award 0622133, ONR Award N000140811014, and Peregrine Semiconductors. This paper was recommended by Associate Editor M. Stanaćević.

D. Kim was with the Department of Electrical Engineering, Yale University, New Haven, CT 06520 USA. He is now with Aptina Imaging, San Jose, CA 95134 USA (e-mail: dongsoo@gmail.com).

B. Goldstein and W. Tang are with the Department of Electrical Engineering, Yale University, New Haven, CT 06520 USA (e-mail: brian.goldstein@yale.edu; wei.tang@yale.edu).

F. Sigworth is with the Department of Biomedical Engineering, Yale University, New Haven, CT 06520 USA (e-mail: fred.sigworth@yale.edu).

E. Culurciello is with the Department of Biomedical Engineering, Purdue University, West Lafayette, IN 47907 USA (e-mail: euge@purdue.edu).

Color versions of one or more of the figures in this paper are available online at http://ieeexplore.ieee.org.

Digital Object Identifier 10.1109/TBCAS.2012.2192273

sensing elements. Inductors can also be used for large AC currents, but are not generally employed in biosensor interfaces for their size and the small currents involved [14]. Although the shunt structures provide a simple implementation, they cause a high offset voltage error and can not provide a clamping voltage. Therefore, typical systems use an operational amplifier with capacitive [12], [13] or resistive feedback [1] as a head-stage. Another approach is using a current amplifier to amplify the input current eliminating the noise sources from the following stages [9], [10], [15]. An ideal low-current measurement system provides the following features: measures low-current with the maximum bandwidth and sensitivity available, allows measurement of bidirectional currents (sinking/sourcing), and allows control of the voltage at the input node (voltage clamping). Note that there is always a tradeoff between noise performance and bandwidth [16].

This paper provides an extensive circuits and systems review of LCMSs and also summarizes a detailed theoretical analysis of their noise performance. The purpose of this paper is to illustrate the proper low-noise design methodology for a state-of-the-art LCMS implemented using current CMOS technologies. We analyze and compare three different kinds of integrated low-current measurement systems: a resistive feedback system, a capacitive feedback system, and a current amplifier system. Section II describes fundamentals of noise analysis and characteristics of the input equivalent circuits used in the previously mentioned applications. Detailed noise analysis of the resistive feedback, capacitive feedback and current amplifier LCMSs will be discussed in Section III. The noise performance comparison and the measurement results of the fabricated LCMSs are presented in Section IV. Finally, the conclusion is provided.

II. Noise Analysis of Input Equivalent Circuits

A. Conventions on Noise Analysis

In electronic circuits, there are a variety of noise sources that degrade the system performance including thermal noise, shot noise, flicker noise, and environmental noises. Here, we summarize our conventions on equations and formulas used throughout the paper to model noise in LCMSs. We use conventional formulas for shot, flicker and thermal noise found in reference [17].

A high-performance operational amplifier (op-amp) is the fundamental building block for a voltage-clamping current measurement system. The role of the op-amp as a transconductor makes its noise performance critical for the overall noise performance of the system. An op-amp can be modeled as an input-referred voltage noise source, e_M and a noiseless op-amp. The noise model of the op-amp used in this analysis is given in (1)

$$\begin{aligned}\overline{e_M^2} &= \overline{V_{n,thermal}^2} + \overline{V_{n,flicker}^2} \\ &= \frac{2 \cdot 8KT}{3 \cdot g_m} + \frac{2}{g_m^2}\left[\frac{K_F \cdot I_D^{AF}}{C_{OX} L_{eff}^2 f}\right]\left[\frac{V^2}{Hz}\right]. \end{aligned} \quad (1)$$

However, the noise model in (1) is complicated by the amount of free parameters and is too difficult to be used for the basic equation of more complicated circuits. Therefore, we use the simplified as follows:

$$\overline{e_M^2} = C_{TN} + \frac{C_{FN}}{f} \quad \left[\frac{V^2}{Hz}\right] \quad (2)$$

where C_{TN} is the summed coefficient of the thermal noises, and C_{FN} is the summed coefficient of the flicker noises in the op-amp. This simplified equation is used for noise analysis throughout the rest of this paper. From the experimental result with the fabricated op-amp, the coefficients, ($C_{TN} = 1.49\text{e}-15\ [V^2/Hz]$, $C_{FN} = 3.1\text{e}-11\ [V^2]$) can be calculated based on Silicon-on-Sapphire (SOS) 0.5 μm process which is used for different systems to be compared in this paper.

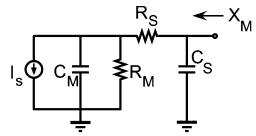

	Cell+Pipette	Patch+Pipette	Cell+Planar	DNA
R_M	500 MΩ	10 GΩ	1 TΩ	1GΩ
C_M	10 pF	200 fF	1-5 fF	60 pF
R_S	5 MΩ	5 MΩ	10 MΩ	1 KΩ
C_S	1 pF	1 pF	100-300 fF	1 pF
I_{in}	10pA-10nA	1-50pA	1-300pA	1-100pA
F_s	5-10KHz	10KHz	10KHz	10KHz

Fig. 2. Schematic diagram of the equivalent input circuit and the electrical values of the equivalent circuit parameters for various biomedical application of the low current measurement systems. Cell+Pipette: whole-cell recording using a micropipette [20], [21], Patch+Pipette: patch-clamp recording using a standard glass micropipette [20], [21], Cell+Planar: whole-cell planar patch-clamp recoding [22], DNA: DNA nanopore sequencing [2], [23]. Current ranges and the sampling frequencies can be different by systems and specified materials to be measured, lower current range and higher sampling frequency are always under research.

B. Equivalent Input Circuit

LCMSs are designed to measure an input current, I_S, with minimum readout current noise. The equivalent input circuit model widely used in biological measurement from cell membranes or nanopores is given in Fig. 2. As can be seen in Fig. 2, a complex impedance model is always present between I_S and the measurement system. This is the impedance of the biological preparation, solutions and measuring electrodes. This input circuit can not only generate considerable input noise, but also changes the overall system performance of the LCMS which affects the noise performance of the system, therefore it is important to analyze it together with the entire measurement system. Typically, an electrode is used to access the electrical measurement from cells or tissue, and therefore an access series resistance, R_S, and parasitic capacitance of the electrode at the input node of the LCMS, C_S, are presented in the electrical equivalent input model. In parallel to I_S, a cell or tissue capacitance, C_M, is present. In addition, a shunt resistance, R_M, is the off resistance of the cell or tissue. R_M directly affects the minimum current measurable, as it produces a leak shunt current. More complex models targeted to limitations of biosensors in aqueous

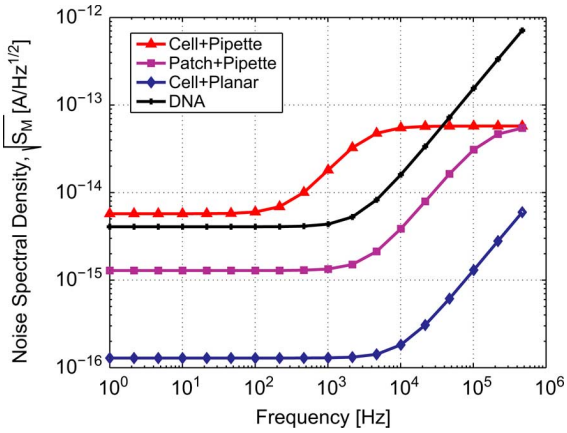

Fig. 3. Electrical characteristic of various cells, membranes and electrodes: Noise spectral density function of the input equivalent circuits.

solutions are available in the literature [18], [19], but are not relevant here, because the complex electrode model is too complicated when it is combined with measurement system analysis. Therefore the simple models provided here capture all essential noise components for this paper and analysis.

Typical electrical parameter values of the equivalent electrical input circuit for common biomedical applications such as whole-cell recording using a micropipette, patch-clamp recording using a micropipette, whole-cell planar patch recording, and DNA nanopore sequencing are given in the table of Fig. 2.

The equivalent impedance of the equivalent input circuit, X_M is defined as

$$\begin{aligned} X_M &= \frac{R_M + R_S + s \cdot R_M \cdot C_M \cdot R_S}{1 + a \cdot s + b \cdot s^2} \\ a &= R_M \cdot C_M + C_S \cdot R_M + C_S \cdot R_S \\ b &= R_M \cdot C_M \cdot R_S \cdot C_S \end{aligned} \tag{3}$$

where C_S is ignored in DNA the nanopore case.

The power spectral density (PSD) of the current noise at X_M, $S_M(f)$ can be calculated as

$$S_M = \frac{4KT}{\mathrm{Re}\{X_M\}} \left[\frac{A^2}{Hz}\right]. \tag{4}$$

We have analyzed the magnitude of the admittance of the input equivalent circuits for various cell membranes and nanopores. The noise spectral density of their complex impedance are presented in Fig. 3. The input equivalent circuit not only generates considerable noise, but also modifies the frequency response of the input-referred noise source of the op-amp, ${e_M}^2$, by the admittance. The cell capacitance, C_M, and the parasitic capacitance, C_S, increase the magnitude of the admittance at higher frequencies. Thus, the multiplication of the admittance and the input referred noise of the op-amp results in an overall input-impedance current noise which has to be much smaller than the input current I_S. The DNA nanopore case is the most challenging application analyzed here, due to the large cell membrane capacitance.

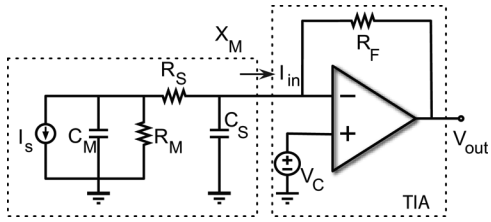

Fig. 4. Schematic of the low current measurement circuit with resistive feedback. X_M is the equivalent input impedance described in Section II-B.

III. Detailed Noise Analysis of Various Low Current Measurement Systems

In this section we will analyze three different low-current measurement systems, based on different headstage circuits. In Section III-A we will present a low-current measurement system with resistive feedback, in Section III-B with capacitive feedback, and in Section III-C a system with a current conveyor as a headstage. In all of these systems, we assume that the goal is to measure an input current, I_{in}, and also provide a voltage control, V_C, to the input current terminal. We also take into account the input impedance model described in Section II-B.

A. Low-Current Measurement With Resistive Feedback

The most typical continuous-time current-mode interface is a resistive feedback trans-impedance amplifier (TIA) based on an operational amplifier headstage [24]–[26]. The resistive feedback TIA is presented in Fig. 4 together with the input equivalent circuit. The operational amplifier input configuration allows to concomitantly record input currents and also clamp the input voltage, V_C. The input is provided through the negative operational amplifier terminal and the voltage-clamp is provided by the virtual short between the two input terminals of the operational amplifier in this configuration. The offset voltage caused by the op-amp itself can be considered part of the offset of the clamping voltage, V_C, and it can be removed by offset subtraction. However the change of the clamping voltage due to the finite gain of the op-amp affects the measurement and it is difficult to remove. The resistive feedback TIA output can measure the input current by means of the relation

$$V_{out} = -I_{in} \cdot R_F. \tag{5}$$

The noise model for the low current measurement system with resistive feedback is presented in Fig. 5 [26]. The noise sources of the resistive feedback system are the feedback resistor and the transistors in the op-amp, and the input impedance presented in the previous section. The output power spectral density, S_V, of the current measuring TIA is given by the equation below

$$S_V = e_R^2 + e_M^2 \cdot (1 + Y_M \cdot R_F)^2 \left[\frac{V^2}{Hz}\right] \tag{6}$$

where e_M is the input referred noise of the op-amp including the thermal and flicker noises, e_R is the thermal noise of the feedback resistor, R_F, and Y_M is the admittance of the equivalent input circuit (cells, membranes and tissues). Note that in this

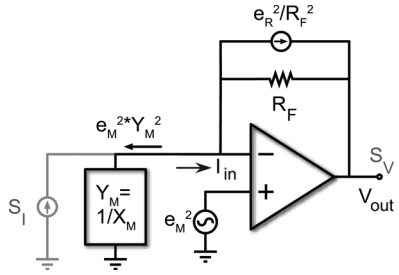

Fig. 5. Noise model for the resistive feedback system.

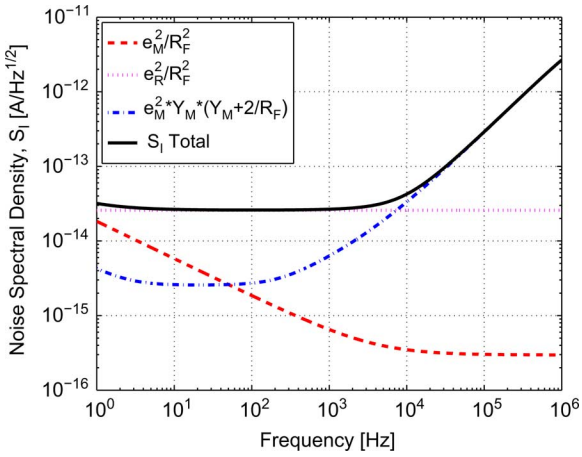

Fig. 6. Current noise spectral density caused by the feedback resistor and the intrinsic op-amp noise in the resistive feedback system for the application in DNA nanopore sequencing.

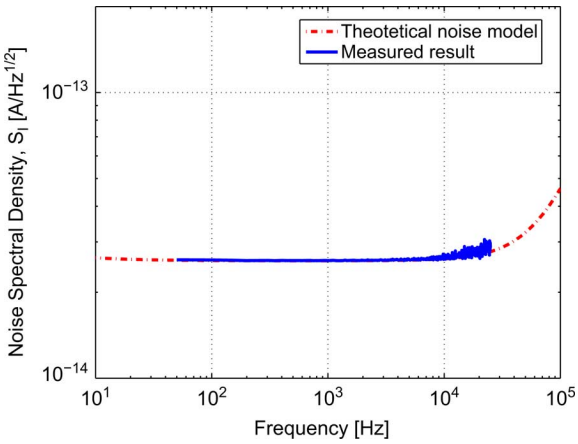

Fig. 7. Current noise spectral density or a resistive feedback LCMS. The theoretical analysis matches the measured results from a fabricated prototype [26], [27] with $R_M = 1\ \mathrm{G\Omega}$ and $C_S = 20\ \mathrm{pF}$.

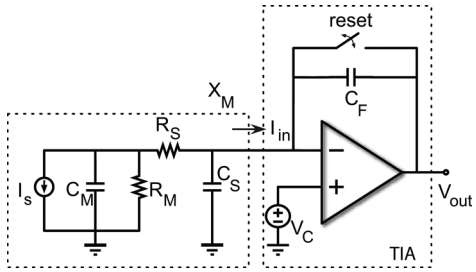

Fig. 8. Schematic of the low current measurement circuit with capacitive feedback.

theoretical analysis we neglect to include the shot noise contribution of the input current to only focus on computing the added noise from electrodes and circuits. We will add shot noise contributions to the model to match with real-case measurements in Section IV.

From the above equations, the power spectral density of the input referred current noise, S_I, can be obtained (7), dividing S_V by R_F^2

$$S_I = \frac{e_M^2 + e_R^2}{R_F^2} + e_M^2 \cdot Y_M \cdot \left(Y_M + \frac{2}{R_F}\right) \left[\frac{A^2}{Hz}\right]. \quad (7)$$

Fig. 6 presents the power spectral response S_I (7) from a LCMS system used for patch-clamp experiments and with a 25 MΩ feedback resistor R_F [25]. The dominant noise source at lower frequencies is the thermal noise of the feedback resistor and the input referred op-amp noise reflected in the admittance of the equivalent input circuit. Notice that this is the highest noise component above 10 kHz. The total input-referred current noise of the low-current measurement system with resistive feedback in Fig. 6 includes the equivalent input circuit of the DNA nanopore (4), and the feedback resistor and the op-amp intrinsic noise (7).

The noise model of the resistive feedback system is matched with the experimental results as follows Fig. 7 (the solid line in Fig. 4 is the dotted line in Fig. 7 as theoretical input referred current noise). This data was collected by a resistive transimpedance amplifier previously published [27], and an input circuit with $R_M = 1\ \mathrm{G\Omega}$ and $C_S = 20\ \mathrm{pF}$.

B. Low-Current Measurement With Capacitive Feedback

A current integrator circuit can be used for low-current integrated measurement systems with larger bandwidth, because the resistive feedback system has a limited bandwidth due to the big feedback resistor which is one of the dominant noise sources. Several implementations of current integrators have been proposed as potentiostats [6], [8], [28]–[30], but none of these provided matching measured noise results to confirm the noise models. This is one of the goals of this paper. Reference [8] provides a noise model that is similar to what is provided here.

The integrator, portrayed in Fig. 8, is a high gain amplifier with a shunt integrating capacitor, C_F, between its input and output terminals. The output voltage of the current integrator is proportional to the integration time and the input current.

Every time the capacitive feedback system is sampled, its operation can be divided in two phases: the *reset* and *integration* phases. In order to analyze in detail the noise performance of the capacitive feedback LCMS we need to separately calculate the noise for both of these operation phases. Here we ignore the switching noise of the feedback capacitor (kT/C noise) and assume this is canceled by correlated double sampling (CDS). But notice that the use of CDS will double the reset thermal noise and any integration thermal noise.

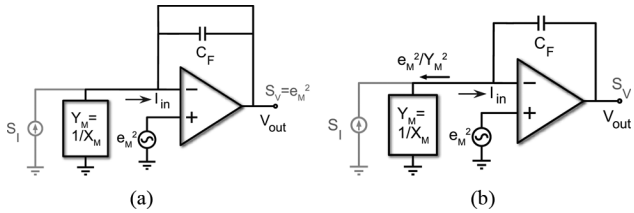

Fig. 9. Noise model for the capacitive feedback system during the reset phase and the integration phase. (a) Reset phase. (b) Integration phase.

During the *reset* phase, the feedback capacitor's terminals are shorted, configuring the op-amp as a voltage follower, as shown in Fig. 9. Thus, the only noise source is the operational amplifier e_M. In this phase, the voltage power spectral density of the output equivalent voltage noise, $S_{V,rst}$ is calculated as

$$S_{V,rst} = e_M^2 \left[\frac{V^2}{Hz}\right] \tag{8}$$

where e_M is the input referred noise of the op-amp. The equivalent input referred current noise, $S_{I,rst}$ related with the feedback capacitance and the integration time can be obtained as

$$S_{I,rst} = S_{V,rst} \cdot \left(\frac{C_F}{T_{int}}\right)^2 \left[\frac{A^2}{Hz}\right]. \tag{9}$$

After reset, the feedback capacitor initial charge is zero. During the *integration* phase, the feedback capacitor integrates the input current, and the integrated output voltage during an integration time, T_{int}, can be represented by a convolution with the current and a rectangular time pulse.

The Laplace transform of $V_{out}(t)$ can be obtained as

$$\mathcal{L}(V_{out}(t)) = \frac{1}{C_F \cdot s} \cdot I_{in}(s) \cdot (1 - e^{-T_{int} \cdot s}) \tag{10}$$

where $L(i(t)) = I_{in}(s)$.

The frequency response of the capacitive integrator during an integration time T_{int} is shown in Fig. 10. The response during the finite time is the combination of two terms: the current integration on the capacitor assuming infinite time (1/s) and the (1—exponential) term. The plot shows both the 1/s term and also the second term with two values of T_{int}: 1 ms and 100 μs. The final frequency response (solid trace with $T_{int} = 100$ μs) is similar to a single-pole low-pass-filter.

From (10), the power spectral density of the output, S_V, is calculated as

$$S_{V,int} = e_M^2 \cdot \left(\frac{Y_M}{C_F \cdot s} \cdot (1 - e^{-T_{int} \cdot s})\right)^2 \left[\frac{V^2}{Hz}\right] \tag{11}$$

where Y_M is the admittance of the equivalent input circuit, X_M.

From the above equations, the input referred current noise during integration, $S_{I,int}$, is

$$S_{I,int} = S_{V,int} \cdot \left(\frac{C_F}{T_{int}}\right)^2$$

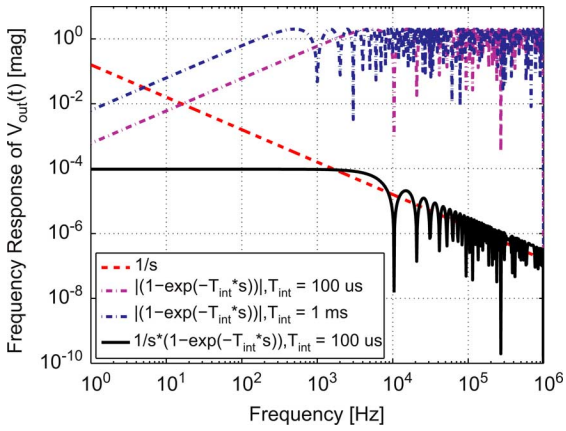

Fig. 10. Frequency response of the capacitive integrator $V_{out}(t)$ during an integration time, T_{int} (solid trace with $T_{int} = 100$ μs). The response during the finite time is the combination of two terms: the current integration on the capacitor assuming infinite time (1/s) and the 1—exponential term, here presented with two values of T_{int}: 1 ms and 100 μs.

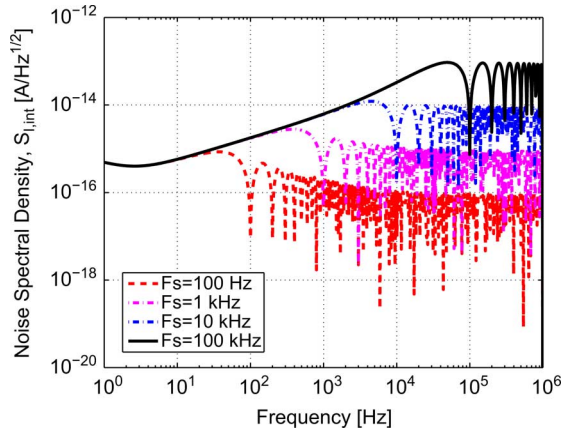

Fig. 11. Current noise spectral density of the integration phase for capacitive feedback system with different sampling frequencies, F_S.

$$= e_M^2 \cdot \left(\frac{Y_M}{T_{int} \cdot s} \cdot (1 - e^{-T_{int} \cdot s})\right)^2 \left[\frac{A^2}{Hz}\right]. \tag{12}$$

The input referred current noise during integration, $S_{I,int}$, is plotted in Fig. 11 for a sampling frequency, F_S, of 100 Hz, 1 kHz, 10 kHz and 100 kHz.

The total input referred noise, S_T of the capacitive feedback measurement system is approximated as the sum of the noise current power spectral densities of the reset phase and the integration phase including the noise of the input equivalent circuit: $S_T = S_M + S_{I,rst} + S_{I,int}$. The noise components and the total noise is plotted in Fig. 12.

When a integrated system is implemented with a switch capacitor circuit, the performance is degraded by switching effects including clock feedthrough, charge injection, and KT/C noise. The correlated double sampling can eliminate effectively the degradation caused by the offsets (clock feedthrough, signal independent charge injection and KT/C) and the low frequency noises. A common CDS circuit is presented in Fig. 13(a), it is connected with the integrator. In high phase of p1 signal, the CDS circuit samples the reset output voltage of the integrator. The integrated signal is subtracted with the stored reset value

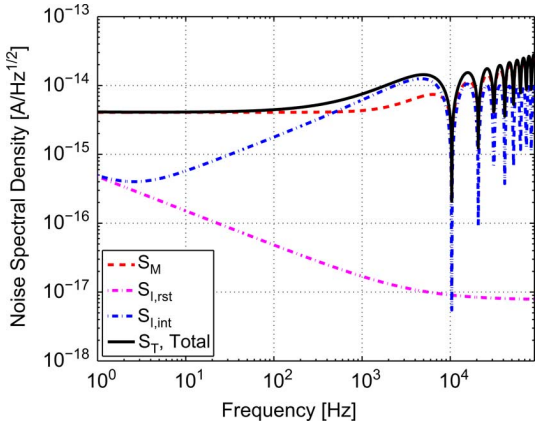

Fig. 12. Total current noise spectral density for capacitive feedback system with $T_{int} = 100\ \mu$s.

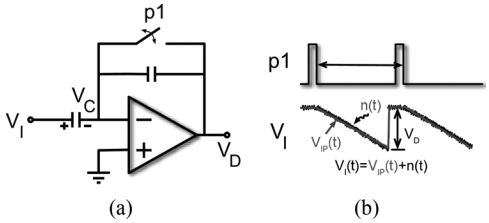

Fig. 13. Schematic diagram of a CDS circuit and waveforms. (a) Schematic of a Correlated Double Sampling (CDS) Circuit. (b) Waveform.

to get the pure integrated signal in the next phase. The output signal of the integrator (input of CDS circuit), $V_I(t)$ includes the noiseless signal $V_{IP}(t)$ and a noise signal $n(t)$. When the reset voltage is sampled in the capacitor in the very short phase of the sampling, the stored noise voltage of the sampling capacitor, $V_C(t)$ can be represented as

$$V_C(t) = \sum_{k=-\infty}^{\infty} n(k \cdot T_S) \cdot h(t - k \cdot T_S)$$
$$h(t - k \cdot T_S) = u(t - k \cdot T_S) - u(t - (k+1) \cdot T_S) \quad (13)$$

where $u(t)$ is the unit step function. When the only noise component of the signal, V_D after CDS is defined as $y(t)$, $y(t)$ can be presented as

$$y(t) = n(t) - \sum_{k=-\infty}^{\infty} n(k \cdot T_S) \cdot h(t - k \cdot T_S). \quad (14)$$

The Fourier Transform, $\mathcal{F}$ of $y(t)$ and $n(t)$ are $Y(j\omega)$ and $N(j\omega)$, respectively. Equation (14) is calculated as follows:

$$Y(j\omega) = N(j\omega) - \mathcal{F}\left\{\sum_{k=-\infty}^{\infty} n(t) \cdot \delta(t - k \cdot T_S)\right\} \cdot \mathcal{F}\{u(t) - u(t - T_S)\}. \quad (15)$$

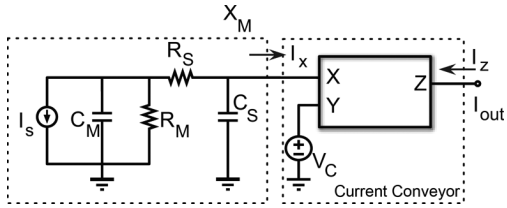

Fig. 14. Schematic of low current measurement circuit with current conveyor.

Based on the properties of the Fourier Transform [31], (15) can be calculated as

$$Y(j\omega) = N(j\omega) \cdot H(j\omega) \quad (16)$$
$$Y(j\omega) = N(j\omega) - sinc\left(\frac{\omega \cdot T_S}{2}\right) \cdot e^{-j \cdot T_S/2\omega} \cdot \sum_{m=-\infty}^{\infty} N\left(j\omega - m \cdot \frac{2\pi}{T_S}\right) \quad (17)$$

where

$$H(j\omega) = \begin{cases} 1 - sinc(\frac{\omega \cdot T_S}{2}) \cdot e^{-j \cdot T_S/2\omega} & \text{if } m = 0 \\ sinc(\frac{\omega \cdot T_S}{2}) \cdot e^{-j \cdot T_S/2\omega} & \text{if } m \neq 0. \end{cases}$$

When CDS is applied with the capacitive feedback system, the low frequency noise (flicker noise) is reduced by the subtraction operation. Whereas the effect of the flicker noise is dramatically reduced by CDS, the thermal noise is increased because the thermal noise is not correlated and the noise is doubled by the subtraction. Therefore, it is important to design the op-amp to have low noise at high frequencies by reducing the thermal noise of the transistors in order to implement an LCMS that has high performance.

C. Low-Current Measurement With Current Conveyor

A current conveyor circuit can amplify low current while applying voltage biases for biosensor interfaces [7], [32]. Fig. 14 presents a schematic of a typical current conveyor used for measuring small currents without the use of operational amplifiers.

The current conveyor circuit performs decoupling and linear operations in current mode in the same way that the operational amplifier performs in voltage mode. The conveyor can decouple the input current and give current amplification, allowing designers to relax both the noise and performance specifications of the following measuring stages. Because the potential of node X is the same with that of node Y, the current conveyor can apply a clamping voltage as is necessary to measure low currents [33]. Notice that the output is a current instead of a voltage, unlike resistive or capacitive feedback systems. Alternatively, if a current mode analog-to-digital convertor (ADC) is used, the current conveyor can perform low-current measurements without additional circuits.

A schematic of the current conveyor circuit is given in Fig. 15. For simplicity all devices have the same size: W, L (width, length) in the input stage and W_2, L in the output stage. If a potential is applied to terminal X, the same potential appears on terminal Y. The current following into terminal X

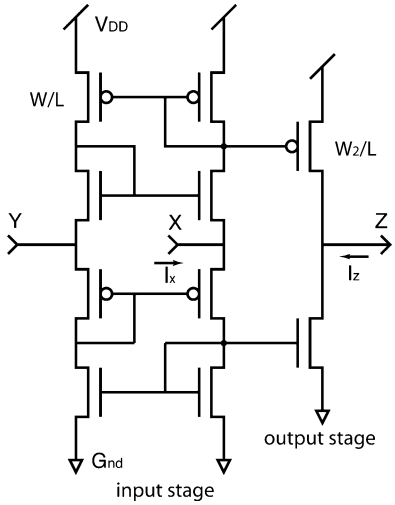

Fig. 15. Schematic circuit of a current conveyor. The input stage implements two latched current mirrors both with PMOS and NMOS transistors. The output stage can provide amplification if the transistor widths are larger than the input ones.

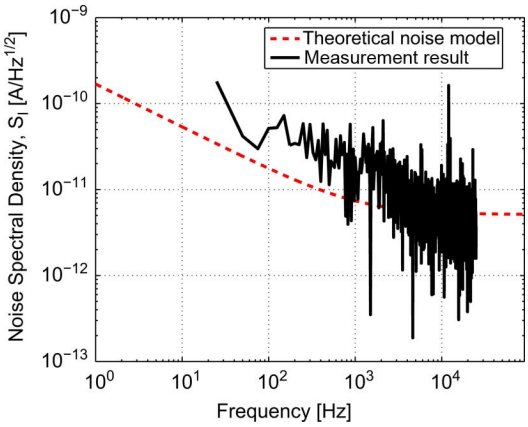

Fig. 16. Current noise spectral density of the current conveyor LCMS. The theoretical noise analysis matches the measured results from an fabricated device in a SOS $0.5\ \mu\mathrm{m}$ process.

will be conveyed into terminal Z with high output impedance. The potential at X is independent of the current flowing and any current flowing into X will flow into Y as well. By inspecting Fig. 15 one can easily determine that all of the above conditions are satisfied by the nature of the input stage and its current mirrors.

The circuit is operated with X as the input port and Z as the output port. Z will act as a current source mirroring the value of the current into X. The output current from Z can be measured by means of the integrative or continuous head stages. Notice that the input current can be amplified using this circuit by making the output stage transistors (right-most transistors in Fig. 15) a factor α times wider than the input stage transistors: $W_2 = \alpha W$. Multiple current mirror stages can also be cascaded to obtain large amplifications of the input current.

Since the input and output of the current conveyor are currents, the input referred current noise can be calculated as

$$S_I = 8 \cdot \left(4KT\frac{2}{3}g_m + \frac{K_F I d^{A_F}}{C_{OX}(L^2)f}\right) + \frac{2}{\alpha} \cdot \left(4KT\frac{2}{3}g_m + \frac{K_F I d^{A_F}}{C_{OX}(L^2)f}\right) \quad (18)$$

$$= \left(8 + \frac{2}{\alpha}\right) \cdot \left(4KT\frac{2}{3}g_m + \frac{K_F I d^{A_F}}{C_{OX}(L^2)f}\right) \left[\frac{A^2}{Hz}\right] \quad (19)$$

where g_m is transconductance of transistors in the input stage α is current amplification factor.

We have fabricated a current conveyor circuit in a $0.5\ \mu\mathrm{m}$ silicon-on-sapphire (SOS) technology. Fig. 16 presents the matching results between the theoretical analysis and measured result. The device reported an rms current noise of 750 pA with a bandwidth of 10 kHz. All parameters in (19) were extracted from the SOS process manual and simulator [14]. This result is similar to the data reported with a lower-noise current conveyor circuit based on operational amplifiers [7]. In the current conveyors, the input signal current from the sensor is merged with the bias current of the conveyor itself. At this point the noise is the overall noise resulting from the sum of the sensor current plus conveyor bias current. Therefore the total noise is huge compared to the resistive or capacitive feedback system which have noise from the sensor alone. For this reason this circuit is not generally used in very low-current measurement systems.

IV. Noise Performance Comparison of the Low-Current Measurement Systems and Their Measured Results

We have fabricated and tested all three different low-current measurement systems presented in Sections III-A–III-C. Low-current measurement systems with resistive feedback [24], [25], capacitive feedback [34]–[37], and a current conveyor [14] were fabricated and tested, and the noise performance of each was reported.

Fig. 17 reports the comparison of the theoretical noise performance of low-current measurement systems for the applications presented in Section II-B. Fig. 17(a) is for whole-cell (nA level currents) patch-clamping using a pipette electrode [20], [21], Fig. 17(b) is for patch-clamping with a pipette and pico-ampere level currents [20], [21], Fig. 17(c) is for whole-cell patch-clamping with a planar low-noise electrode [22], and Fig. 17(d) is for the DNA nanopore sequencing applications with pico-ampere current levels [2]. As can be seen in Fig. 17, the different characteristics of the input equivalent circuit generate different noise responses for each LCMS. The most important result of this paper is that, overall, the current conveyor shows the worst performance across all applications, while the resistive and capacitive feedback case provide state-of-the-art performance, with the capacitive system being slightly better in each case. When used in patch-clamp recording and DNA sequencing applications, both requiring pico-ampere level measurements, the capacitive feedback system is better than the resistive feedback system. Moreover, the capacitive feedback system is much better when used for whole-cell planar patch-clamping, due to the reduced noise of the input admittance in this input configuration. For whole-cell patch-clamping, the performance of the capacitive feedback and the resistive feedback are similar when

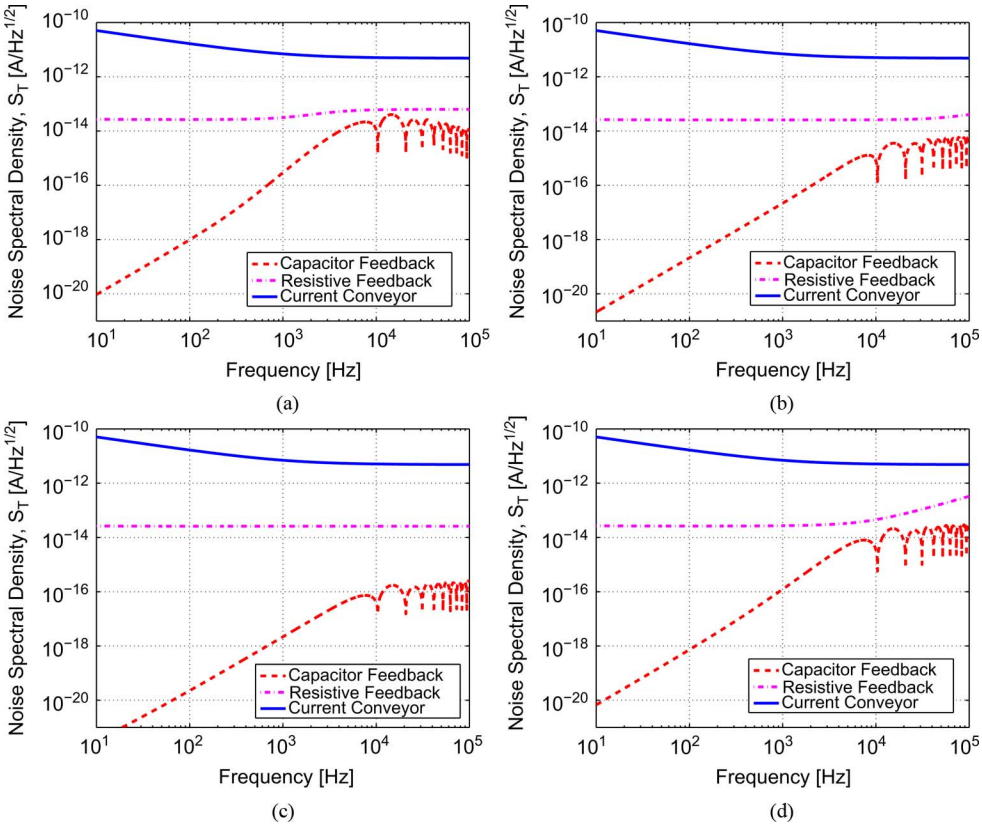

Fig. 17. Current noise spectral density comparison for resistive feedback, capacitive feedback (using CDS), and current conveyor system on various applications, based on the low noise op-amp with the thermal noise level of about $5\ \mathrm{nV}/\sqrt{Hz}$. (a) Whole Cell Recording (Cell+Pipette). (b) Patch-Clamp Recording (Patch+Pipette). (c) Whole cell planar recording (Cell+Planar). (d) DNA sequencing (DNA napore).

high sampling rates are desired, because the high frequency noise is the dominant component of the overall RMS noise current. As reported in Section II-B, the input equivalent circuit of a whole cell measurement generates the highest noise in the frequency range of 1 kHz to 10 kHz. This can also be seen in Fig. 3. We remind the reader that the input parasitic and cell capacitances increase the noise spectral density in the higher frequency as seen in Fig. 3. The thermal noise at the input of the headstage is reflected in this input circuit admittance. The headstage noise is higher in a resistive feedback headstage, since the dominant noise of the resistive feedback system is the thermal noise of the feedback resistor. Note that the input headstage noise of the capacitive feedback headstage is lower, especially when CDS is employed. The large noise added from the input equivalent circuit is the reason why the capacitive feedback and the resistive feedback systems have a similar performance in the higher frequencies. Fig. 18 reports the noise analysis comparison for LCMSs matched with measurement results from the fabricated systems. The measured noise spectral densities of the resistive feedback and the current conveyor are around 2×10^{-14} and 1.3×10^{-12} $[A/\sqrt{Hz}]$ at the maximum bandwidth frequency of 10 kHz, respectively. However, the analysis of capacitive feedback system shows the noise spectral density of 1×10^{-14} $[A/\sqrt{Hz}]$. From the measurement results, we see the measured RMS noise of the capacitive feedback system is 110 fA RMS (calculated) and 750 fA RMS (measured) at a 10 kHz sampling rate, whereas the measured RMS noises of the resistive feedback and the current conveyor are 4 pA and 600 pA with a bandwidth of 10 kHz, respectively. Since the dominant noise source of the resistive feedback is the thermal noise of the feedback resistor, the measured results matched well with the noise analysis. However, the measured RMS noises are slightly higher than the theoretical analysis values due to the signal dependent switching effect and the mismatch of noise parameters in the cases of the capacitive feedback and current conveyor systems. Nevertheless, the noise analysis presented here gives very good matching results.

Recently, we have fabricated an optimized synchronous LCMS with capacitive feedback based on the noise analysis comparison reported in this paper. The optimized LCMS using capacitive feedback was designed and fabricated in a CMOS $0.5\ \mu\mathrm{m}$ process, since the SOS process has higher low frequency noise (flicker noise) than the CMOS process. The circuit and layout of this system are shown in Fig. 19. The fabricated LCMS has two channels, a selectable 100 fF or 1 pF feedback capacitor, and each channel occupies $630 \times 220\ \mu\mathrm{m}^2$. The LCMS noise performance was tested using precisely known currents by applying voltage over a 10 GΩ resistor using a Keithley 236 Source Measure Unit. For this test we used a 100 fF integration cap, a 10 kHz sampling rate, and we did not filter the output voltage (worst case scenario). The input capacitance of the system packaged in a circuit board and with the 10 GΩ resistor was estimated to be 8 pF. The current noise spectral density and measurement results of the synchronous

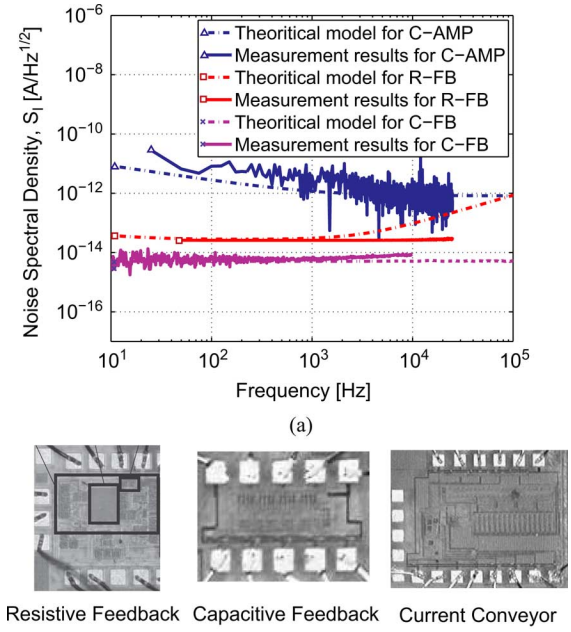

Fig. 18. (a) Current noise spectral density comparison and the matched measurement results and microphotographs of LCMSs fabricated with SOS $0.5\ \mu$m process for (b) Resistive Feedback (R-FB), Capacitive Feedback (C-FB), and Current Conveyor (C-AMP) systems. Theoretical models and the measurement results are normalized with the power consumption of 1 mA at 3.3 V for the fair comparison.

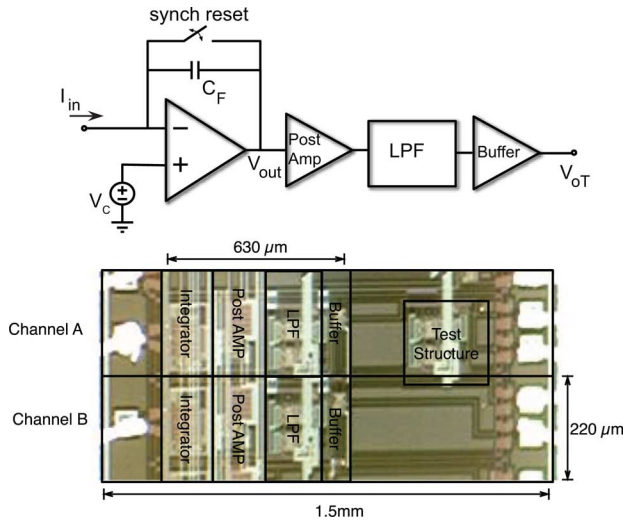

Fig. 19. Low current measurement system using the capacitive feedback with CMOS $0.5\ \mu$m process.

capacitive feedback LCMS from Fig. 19 and the model from (12) is shown in Fig. 20.

Fig. 21 shows the theoretical model and the measurement results. Compared to the theoretical results in Fig. 17, here we used a model that takes into account the shot noise of the leakage current at the input of the integrator, the ADC quantization noise, and the output buffer voltage noise contribution. We observed a 20 pA leakage current at the input of the integrator. This leakage is due to the reset transistor across the feedback capacitor C_F. This leakage was externally compensated by adding an identical current. Both these currents contribute to

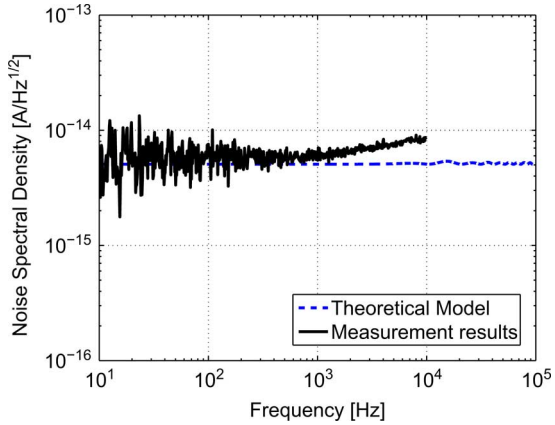

Fig. 20. Current noise spectral density and measurement results of the synchronous capacitive feedback LCMS from Fig. 19 and the model from (12). The added input capacitance was 47 pF, the integration capacitor used was 100 fF, and the recording bandwidth was 10 kHz.

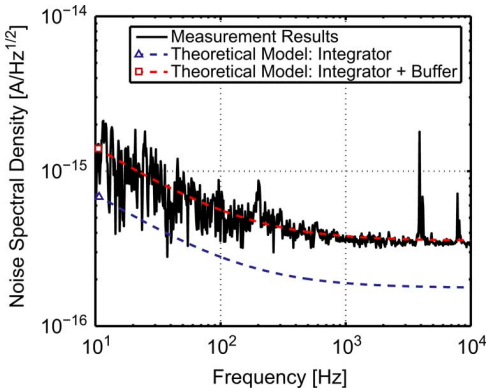

Fig. 21. Current noise spectral density and measurement results of the reset phase of the synchronous capacitive feedback LCMS from Fig. 19 and the model from (9).

shot noise of $3.6\ \mathrm{fA}/\sqrt{Hz}$, and this is one of the largest components in the 10 kHz bandwidth. The ADC used is 16 bits and contributed to $0.145\ \mathrm{fA}/\sqrt{Hz}$. The output buffer has a thermal noise level of $20\ \mathrm{nV}/\sqrt{Hz}$, and its contribution reflected at the input was $20\ \mathrm{aA}/\sqrt{Hz}$. The correlated double sampling (CDS) function was performed by externally double sampling the output voltage in the integration phase to eliminate the offset and low frequency noise. We note that the CDS is not able to reduce the noise added by these three factors, and in actuality in the worst case it doubles them since these noise are uncorrelated between two samples. Finally, note that the $10\ \mathrm{G}\Omega$ resistor noise contribution with CDS is $5.15\ \mathrm{fA}/\sqrt{Hz}$. The measured noise power spectral density is higher than the theoretical model because there is the external noise noise and the mismatch of the noise parameter.

V. Conclusion

Based on the theoretical analysis and the measurement results, the LCMS using capacitive feedback has a lower noise level than the resistive feedback and the current conveyor for the described applications. The performance difference is changed by the characteristics of the input equivalent circuit for each application. The CDS technique and a low-pass filter which

has a bandwidth which can be changed depending on the input signal frequency can increase the noise performance of the synchronous capacitive feedback LCMS. This paper also presents a comprehensive analysis of low-current measurement systems and helps technical personnel, scientists and engineers to design the lowest noise system for biomedical and nano-science applications.

REFERENCES

[1] F. Sigworth and K. Klemic, "Microchip technology in ion-channel research," *IEEE Trans. Nanobiosci.*, vol. 4, pp. 121–127, 2005.

[2] D. Branton *et al.*, "The potential and challenges of nanopore sequencing," *Nature Biotechnol.*, vol. 26, pp. 1146–1153, 2008.

[3] E. Katz and I. Willner, "Probing biomolecular interactions at conductive and semiconductive surfaces by impedance spectroscopy: Routes to impedimetric immunosensors, dna-sensors, and enzyme biosensors," *Electroanal.*, vol. 15, no. 11, pp. 913–947, 2003.

[4] E. Stern, J. Klemic, D. Routenberg, P. Wyrembak, D. Turner-Evans, A. Hamilton, D. LaVan, T. Fahmy, and M. Reed, "Label-free immunodetection with CMOS-compatible semiconducting nanowires," *Nature*, vol. 05498, no. 445, 2007.

[5] R. J. Reay, S. P. Kounaves, and G. T. Kovacs, "An integrated CMOS potentiostat for miniaturized electroanalytical instrumentation," in *Proc. IEEE Int. Solid-State Circuits Conf.*, Feb. 1994, pp. 162–163.

[6] K. Murari, N. Thakor, M. Stanacevic, and G. Cauwenberghs, "Wide-range, picoampere-sensitivity multichannel VLSI potentiostat for neurotransmitter sensing," in *Proc. 26th Annu. Int. Conf. IEEE Engineering in Medicine and Biology Society*, San Francisco, CA, Sep. 2004.

[7] R. Genov, M. Stanacevic, M. Naware, G. Cauwenberghs, and N. Thakor, "16-channel integrated potentiostat for distributed neurochemical sensing," *IEEE Trans. Circuits Syst. I, Reg. Papers*, vol. 53, no. 11, pp. 2371–2376, 2006.

[8] A. Gore, S. Chakrabartty, and E. Alocilja, "A multichannel femtoampere-sensitivity potentiostat array for biosensing applications," *IEEE Trans. Circuits Syst. I, Reg. Papers*, vol. 53, no. 11, pp. 2357–2363, 2006.

[9] G. Ferrari, F. Gozzini, and M. Sampietro, "Very high sensitivity CMOS circuit to track fast biological current signals," in *Proc. IEEE Biomedical Circuits and Systems Conf.*, 2006, pp. 53–56.

[10] G. Ferrari, F. Gozzini, and M. Sampietro, "A current-sensitive front-end amplifier for nano-biosensors with a 2 MHz BW," in *Proc. IEEE Int. Solid-State Circuits Conf., Dig. Tech. Papers*, 2007, pp. 164–165.

[11] M. Stanacevic, K. Murari, A. Rege, G. Cauwenberghs, and N. Thakor, "VLSI potentiostat array with oversampling gain modulation for wide-range neurotransmitter sensing," *IEEE Trans. Biomed. Circuits Syst.*, vol. 1, no. 1, pp. 63–72, 2007.

[12] A. Yang, S. R. Jadhav, R. M. Worden, and A. J. Mason, "Compact low-power impedance-to-digital converter for sensor array microsystems," *IEEE J. Solid-State Circuits*, vol. 44, no. 10, pp. 2844–2855, 2009.

[13] G. Ferrari, F. Gozzini, A. Molari, and M. Sampietro, "Transimpedance amplifier for high sensitivity current measurements on nanodevices," *IEEE J. Solid-State Circuits*, vol. 44, no. 5, pp. 1609–1616, May 2009.

[14] E. Culurciello, *Silicon-on-Sapphire Circuits and Systems, Sensor and Biosensor Interfaces*. New York: McGraw-Hill, 2009.

[15] G. Ferrari, M. Farina, F. Guagliardo, M. Carminati, and M. Sampietro, "Ultra-low-noise CMOS current preamplifier from dc to 1 MHz," *Electron. Lett.*, vol. 45, p. 1278, 2009.

[16] D. Kim, W. Tang, B. Goldstein, P. Weerakoon, and E. Culurciello, "Performance comparison of low current measurement systems for biomedical applications," in *Proc. IEEE Int. Symp. Circuits and Systems*, Paris, France, May 2010.

[17] B. Razavi, *Design of Analog CMOS Integrated Circuits*. New York: McGraw-Hill, 2000.

[18] A. Hassibi, R. Navid, R. Dutton, and T. Lee, "Comprehensive study of noise processes in electrode electrolyte interfaces," *J. Appl. Phys.*, vol. 96, p. 1074, 2004.

[19] A. Hassibi, H. Vikalo, and A. Hajimiri, "On noise processes and limits of performance in biosensors," *J. Appl. Phys.*, vol. 102, no. 1, p. 014909, 2007.

[20] O. Hamill, A. Marty, E. Neher, B. Sakmann, and F. Sigworth, "Improved patch-clamp technique for high-resolution current recording from cells and cell-free membrane patches," *Eur. J. Phys.*, vol. 391, pp. 85–100, 1981.

[21] R. Levi and J. Rae, "Technology of patch-clamp electrodes," *Patch-Clamp Anal.*, pp. 1–34, 2007.

[22] N. Fertig, R. Blick, and J. Behrends, "Whole cell patch clamp recording performed on a planar glass chip," *Biophys. J.*, vol. 82, no. 6, pp. 3056–3062, 2002.

[23] S. M. Iqbal, *Nanopores: Sensing and Fundamental Biological Interactions*. Berlin, Germany: Springer, 2011.

[24] P. Weerakoon, E. Culurciello, Y. Yang, J. Santos-Sacchi, P. Kindlmann, and F. Sigworth, "Patch-clamp amplifiers on a chip," *J. Neurosci. Methods*, vol. 192, pp. 187–192, Oct. 2010.

[25] P. Weerakoon, F. Sigworth, P. Kindlmann, J. Santos-Sacchi, Y. Yang, and E. Culurciello, "An integrated patch-clamp system with dual input," in *Proc. IEEE Int. Symp. Circuits and Systems*, Paris, France, May 2010.

[26] P. Weerakoon, K. Klemic, F. Sigworth, and E. Culurciello, "An integrated patch-clamp potentiostat with electrode compensation," *IEEE Trans. Biomed. Circuits Syst.*, vol. 3, no. 2, pp. 117–125, 2009.

[27] P. Weerakoon, K. Klemic, F. Sigworth, and E. Culurciello, "Integrated patch-clamp biosensor for high-density screening of cell conductance," *Electron. Lett.*, vol. 44, no. 2, pp. 81–82, Jan. 2008.

[28] R. G. Kakerow, H. Kappert, E. Spiegel, and Y. Manoli, "Low power single chip CMOS potentiostat," in *Proc. 8th Int. Conf. Solid-State Sensors and Actuators*, Jun. 1995, pp. 142–145.

[29] A. Bandyopadhyay, G. Mulliken, G. Cauwenberghs, and N. Thakor, "VLSI potentiostat array for distributed electrochemical neural recording," in *Proc. IEEE Int. Symp. Circuits and Systems*, Phoenix, AZ, May 2002, pp. II-740–II-743.

[30] H. Narula and J. Harris, "A time-based vlsi potentiostat for ion current measurements," *IEEE Sensors J.*, vol. 6, no. 2, pp. 239–247, Apr. 2006.

[31] R. Bracewell, "The Fourier transform," *Sci. Amer.*, vol. 260, no. 6, pp. 86–95, 1989.

[32] R. F. Turner, D. J. Harrison, and H. P. Baltes, "A CMOS potentiostat for amperometric chemical sensors," *IEEE J. Solid State Circuits*, vol. 22, pp. 473–478, May 1987.

[33] E. Bruun, "Analysis of the noise characteristics of cmos current conveyors," *Analog Integr. Circuits Signal Process.*, vol. 12, no. 1, pp. 71–78, Jan. 1997.

[34] F. Laiwalla, K. Klemic, F. Sigworth, and E. Culurciello, "An integrated patch-clamp amplifier in silicon-on-Sapphire CMOS," *IEEE Trans. Circuits Syst.*, vol. 53, no. 11, pp. 2364–2370, Nov. 2006.

[35] F. Laiwalla, K. Klemic, F. Sigworth, and E. Culurciello, "An integrated silicon-on-sapphire patch-clamp amplifier," in *Proc. IEEE/NLM Life Science Systems and Application Workshop*, Bethesda, MD, Jul. 2006.

[36] F. Laiwalla, K. Klemic, F. Sigworth, and E. Culurciello, "An integrated patch-clamp amplifier in silicon-on-sapphire CMOS," in *Proc. IEEE Int. Symp. Circuits and Systems*, Kos, Greece, May 2006, pp. 4054–4057.

[37] E. Culurciello, H. Montanaro, and D. Kim, "Ultra-low current measurements with silicon-on-sapphire integrator circuits," *IEEE Electron Device Lett.*, vol. 30, no. 3, pp. 258–260, Mar. 2009.

Dongsoo Kim (M'02) received the M.S. and Ph.D. degrees in electrical and electronics engineering from Yonsei University, Seoul, Korea, in 2004 and 2008, respectively

Currently, he works as a Senior Analog Design Engineer at Aptina Imaging, San Jose, CA. From 2008 to 2010, he was a Postdoctoral Associate in the Department of Electrical Engineering, Yale University, New Haven, CT. His research interests include CMOS image sensors, smart sensors, low-noise circuit design, and biomedical instrumentation.

Brian Goldstein (GS'08) received the B.S. degree in computer and systems engineering and computer science from Rensselaer Polytechnic Institute, Troy, NY, in 2006, and the M.S. and M.Phil. degrees in electrical engineering from Yale University, New Haven, CT, in 2010 and 2011, respectively.

Currently, he is working toward the Ph.D. degree at Yale University. From 2006 to 2008, he worked on embedded systems at Goodrich Pump and Engine Control Systems, N.A., West Hartford, CT. His research interests include analog and mixed-signal integrated circuits, low-noise circuit design, and systems engineering for biomedical applications.

Wei Tang (S'06) received the B.S. degree in microelectronics from Peking University, Peking, China, in 2006.

Currently, he is working toward the Ph.D. degree at Yale University, New Haven, CT. In 2007, he became a Research Assistant in the Yale E-Lab. His research interests are analog/mixed-signal and low-power circuit design, as well as RF/wireless communication circuits and systems design and testing for biomedical applications.

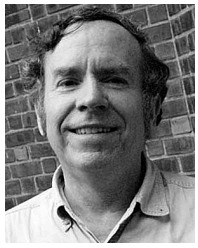

Fred J. Sigworth received the B.S. degree in applied physics from the California Institute of Technology, Pasadena, in 1974, and the Ph.D. degree in physiology from Yale University, New Haven, CT, in 1979.

He has worked in the laboratory of C. F. Stevens at Yale University. He was a Postdoctoral Fellow in the laboratory of E. Neher in Göttingen, Germany. Since 1984, he has been a Faculty Member in the Department of Cellular and Molecular Physiology at the Yale School of Medicine, and holds a joint appointment in the Department of Biomedical Engineering. His research group studies the function and structure of ion-channel proteins.

Eugenio Culurciello (S'97–M'99–SM'11) received the Ph.D. degree in electrical and computer engineering from The Johns Hopkins University, Baltimore, MD, in 2004.

He is an Associate Professor in the Weldon School of Biomedical Engineering, Purdue University, West Lafayette, IN, where he directs the e-Lab laboratory. His research interests include analog and mixedmode integrated circuits for biomedical instrumentation, synthetic vision, bio-inspired sensory systems and networks, biological sensors, and silicon-on-insulator design. He was the recipient of The Presidential Early Career Award for Scientists and Engineers (PECASE) and Young Investigator Program from ONR, the Distinguished Lecturer of the IEEE (CASS), and is the author of *Silicon-on-Sapphire Circuits and Systems, Sensor and Biosensor Interfaces* (McGraw-Hill: New York) in 2009.